**Article:**

Takahagi, K. orcid.org/0009-0003-7592-4216 and Tennant, A. (2025) Near-field characteristic verification for non-reciprocity radome. The Journal of Engineering, 2025 (1). e70096. ISSN 2051-3305

https://doi.org/10.1049/tje2.70096

*The Journal of Engineering*

WILEY

The Institution of Engineering and Technology

ORIGINAL RESEARCH OPEN ACCESS

# Near-Field Characteristic Verification for Non-Reciprocity Radome

Kazuhiro Takahagi | Alan Tennant

Department of Electrical and Electronics Engineering, The University of Sheffield, Sheffield, UK

**Correspondence:** Kazuhiro Takahagi (ktakahagi1@Sheffield.ac.uk)

**Received:** 3 March 2025 | **Revised:** 17 April 2025 | **Accepted:** 12 May 2025

**Funding:** The authors received no specific funding for this work.

## ABSTRACT

We propose a nonreciprocal metasurface designed to suppress reflections in antennas, which have become a major source of electromagnetic interference with the increasing use of electromagnetic waves. A nonreciprocal metasurface capable of controlling transmission and blocking based on the propagation direction can play a crucial role in maintaining antenna performance while mitigating electromagnetic interference. The proposed nonreciprocal structure introduces nonreciprocity by incorporating a magnetic material into a conventional radio wave filter, enabling effective operation in both the far-field and near-field regions. In this study, we verify the near-field operation of a nonreciprocal metasurface, demonstrating an isolation of more than 10 dB at 6.3 GHz using a 6 GHz band antenna. Additionally, we report the effects of the metasurface on the antenna radiation pattern.

## 1 | Introduction

The rapid increase in the use of electromagnetic waves has created a strong demand for precise and intelligent management of electromagnetic fields [1]. This is particularly critical in applications such as communications and radar, where higher frequencies are employed for larger capacities, and higher power is utilized for long-distance propagation. One of the most significant challenges in these scenarios is reducing electromagnetic interference that arises when the frequencies and physical locations of electromagnetic waves are in close proximity [2]. Specific challenges arise in the vicinity of antennas. As antenna apertures increase to enhance performance, they are also being placed in high-density configurations to save space. These antennas not only serve as significant sources of unwanted reflections but also interfere with other electronic devices. To improve the stealth of antenna components and mitigate reflection-induced interference, various physical and electronic countermeasures have been proposed. Physical solutions include optimizing the antenna mounting angle [3] and spatially separating transmitting and receiving antennas [4]. Meanwhile, electronic control techniques, such as null steering in specific directions [5] and interference cancellation methods [6], have also been explored. These existing solutions require advanced control, may constrain antenna performance, and present challenges in space-constrained applications. Recent studies have focused on nonreciprocal metasurfaces, which leverage radio wave properties such as frequency and polarization to achieve nonreciprocity in propagation direction [7, 8]. This enables the transmission of radio waves only in the desired direction while blocking waves from other directions, providing a potential approach for interference suppression. However, in nonreciprocal metasurfaces that incorporate antenna elements or complex-shaped patch elements, it is necessary to separate them into the far-field region, where the waves become plane waves, to fully demonstrate their properties. Consequently, challenges remain in achieving effective operation in the near-field region. On the other hand, radomes with nonreciprocity properties utilizing magnetic materials have been reported [9],

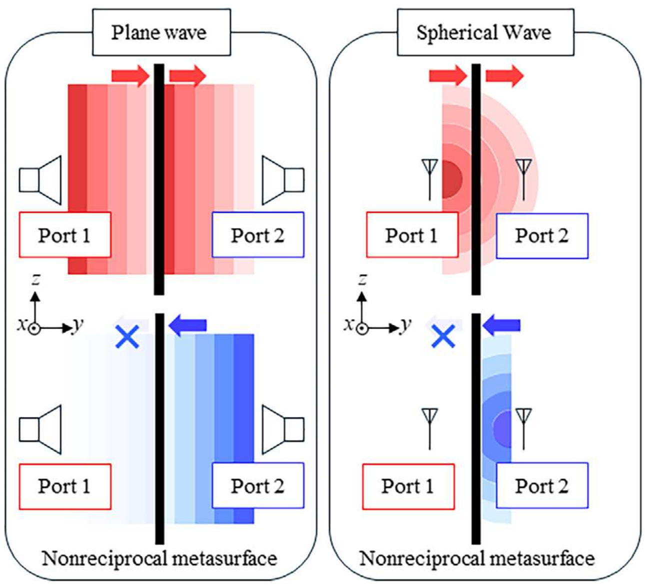


**FIGURE 1** | Definition of a nonreciprocal metasurface for a plane wave in the far field and a nonreciprocal metasurface for a spherical wave in the near field.

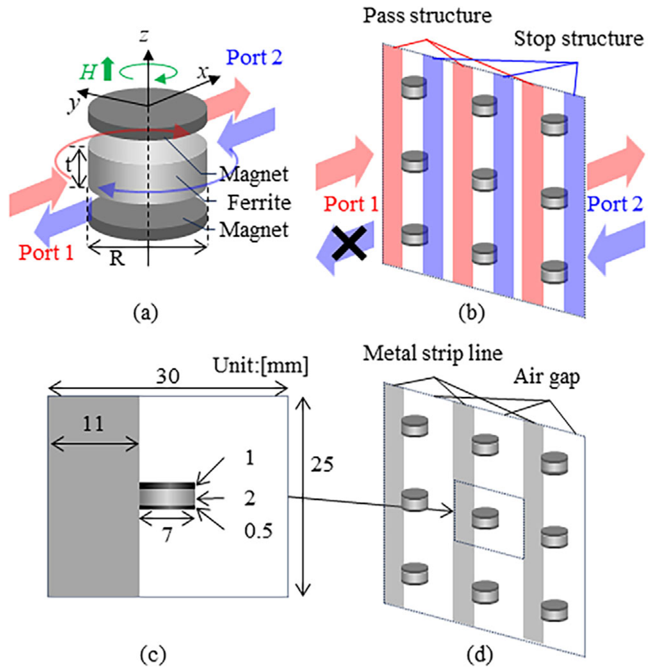


**FIGURE 2** | Nonreciprocal structure: (a) ferrite and magnet configuration; (b) operating principle; (c) unit cell; and (d) nonreciprocal structure applied to antenna.

suggesting their potential to address challenges associated with operation near antennas.

In many studies on nonreciprocal metasurfaces utilizing magnetic materials, magnetization is applied along the radio wave propagation axis [7, 9]. In this approach, nonreciprocity is achieved by altering polarization through the rotational propagation characteristics induced by the anisotropic magnetic permeability of the magnetic material. However, this results in a shift in the polarization of the transmitted wave relative to the incoming wave, posing a challenge. Additionally, the metasurface requires vertical magnetization, which imposes constraints on the magnetization process and magnet placement, making it difficult to flexibly adjust or control the magnetization. To address these challenges, this study aims to achieve nonreciprocity while preserving the characteristics of the incoming wave, including its polarization. Furthermore, we propose a structure that can be easily magnetized, facilitating practical implementation. This approach enables the realization of a nonreciprocal metasurface that functions correctly not only for plane waves but also in proximity to an antenna, as illustrated in Figure 1. The nonreciprocal metasurfaces investigated in this study employ a ferrite magnetized perpendicular to the propagation direction in combination with a metal array pattern. This method offers the advantage of imparting nonreciprocity while preserving the inherent properties of the existing metal array pattern. Moreover, by leveraging the rotational propagation characteristics of magnetic materials, this approach has the potential to exhibit consistent performance in both near-field and far-field regions. This paper presents the optimization of a previously validated structure [10], designed for plane waves in the far field, to ensure proper operation near an antenna. The effectiveness of this optimization is demonstrated through experimental validation and electromagnetic field simulations. Additionally, we investigate methods to actively generate and control null points using a physical radome structure.

The novelty of this study, along with a comparison to previous research, is summarized in Table 1. As previously mentioned, nonreciprocal metasurfaces can be broadly categorized into magnetically biased and non-magnetic types. In magnetically biased approaches, nonreciprocity is achieved by controlling not only the permittivity but also the permeability of the material. In contrast, non-magnetic approaches typically employ planar antennas integrated with nonreciprocal electronic components, forming metasurfaces that function similarly to repeaters. In the present study, as shown in the comparison table, a magnetically biased approach is adopted under the assumption that the metasurface will be used as a radome. This work proposes a structure that simplifies the magnetization process and enhances the controllability of magnetic materials, while also offering polarization flexibility. Furthermore, the proposed design is scalable—not only applicable as a radome for single antennas but also extendable to array antenna systems.

## 2 | Nonreciprocal Structure for Far-Field

### 2.1 | Design of Nonreciprocal Structure

The proposed nonreciprocal metasurface structure consists of a cylindrical ferrite magnetized by upper and lower magnets positioned at the center of a unit cell, flanked by a pass structure and a stop structure on either side, respectively (Figure 2a and b) [10]. Previously reported nonreciprocal metasurfaces using magnetic materials are typically magnetized along the propagation axis [9, 11]. While this approach allows uniform magnetization and a thinner overall structure by reducing ferrite thickness, challenges remain regarding polarization changes during transmission and the stability of magnetization. In contrast, the proposed structure uses ferrite magnetized perpendicular to the propagation axis,

**TABLE 1** | Comparison with previous studies.

| | This work | [9] | [11] | [8] |
|---|---|---|---|---|
| Magnet/non-mag. | M | M | M | N |
| Magnetization controllability | ○ | △ | △ | N/A |
| Radome | ○ | ○ | N/A | N/A |
| Polarization Consistency | ○ | × | △ | △ |
| Arraying | ○ | △ | ○ | ○ |

Abbreviations: ○:Possible, △:Partially possible, ×:Not possible, N/A: Not applicable.

as depicted in Figure 2a. This configuration, proven effective in waveguide and microstrip line circulators [12], integrates ferrite magnetized by upper and lower magnets into a single unit. The rotational propagation characteristics, leveraging the anisotropic magnetic permeability of the magnetized ferrite, allow the pass structure on one side or the stop structure on the other side to dominate, depending on the direction of propagation. This structure supports vertical polarization, where the electric field aligns with the magnetization direction of the ferrite. Horizontal polarization can be achieved by rotating the ferrite and pass structure by 90 degrees. This flexibility ensures nonreciprocal propagation without altering the intrinsic characteristics of the radio wave, such as polarization. Additionally, the ferrite's low projected area ratio (a few percent) minimizes interference with the array structure. To ensure practical applicability, the ferrite in each unit cell is magnetized individually, enabling reliable parallel magnetic fields. The magnets can be either permanent or electromagnetic [13]. With permanent magnets, flipping the ferrite reverses the rotational propagation direction. Electromagnets provide further flexibility by allowing propagation direction changes via current control and enabling ferrite activation or deactivation by toggling the power supply.

The operating band of the antenna in this study is 6 GHz, and a monopole antenna with an isotropic pattern in the horizontal plane serves as the reference. The unit cell's dimensions are determined based on the relationship between the wavelength and the nonreciprocal structure's transmission properties. The ferrite diameter is chosen according to the operating frequency band, as described by Equation (1) [12].

$$R_f = \frac{1.84}{2\pi f_0 \sqrt{\mu_r \varepsilon_r}} \tag{1}$$

Here, $\varepsilon_r$ represents the permittivity, and $\mu_r$ represents the permeability of ferrite. A commercially available circulator (diameter 7 mm, equivalent to G-1600) [14] is used. Optimal unit cell dimensions are calculated as follows: the width includes the ferrite diameter, gap, and metal patch width, while the height slightly exceeds the antenna height. For the 6 GHz band, the unit cell width is set to 30 mm, with a height of 25 mm. The structural design is shown in Figure 2c, and the array structure in Figure 2d. Electromagnetic field analysis using CST Studio Suite validates the design. The array structure is analysed under unit cell boundary conditions in the F-solver module to ensure validity over an infinite plane. The pass structure's filter characteristics are derived from a one-dimensional metal strip line with a width of 11 mm and a pitch of 30 mm, calculated using transmission line theory [15]. The ferrite used in the electromagnetic field simulation is defined as a gyrotropic material, and various parameters are shown in Table 2.

**TABLE 2** | Ferrite parameters used in the electromagnetic field simulation.

| Parameters | Value | Parameters | Value |
|---|---|---|---|
| Relative permittivity | 15 | Relative permeability | 1.1 |
| Rande factor | 2.0 | Saturation magnetization | 1600 Oe |
| Resonance line width | 300 Oe | Magnetic field | 650 Gauss |

The transmission coefficient $S_{11}$ and reflection coefficient $S_{21}$ of the strip line are calculated according to the transmission line theory using Equations (2) to (6). In the case of the strip line, the impedance component Z is only the inductive reactance component $X_L$.

$$X_L \approx \frac{p\, cos\varphi}{\lambda} \left\{ 1n \frac{2p}{\pi d} + \frac{1}{2}\left(3 - 2cos^2\varphi\right)\left(\frac{p}{\lambda}\right)^2 \right\} \tag{2}$$

Here, $p$ is the pitch of the strip line arrays, d is the width of strip line, and phi is the angle of incident.

$$Z = jX_L \tag{3}$$

$$Y = Z^{-1} \tag{4}$$

$$|T|^2 = \frac{4}{4 + |Y|^2} \tag{5}$$

$$S_{11} = 10log\left(1 - |T|^2\right) \tag{6}$$

$$S_{21} = 10log\left(|T|^2\right) \tag{7}$$

First, we analyse the plane wave response of a structure composed solely of ferrite, using the ferrite parameters listed in Table 2. A magnetized ferrite exhibits rotational propagation characteristics for incident electromagnetic waves, while fundamentally allowing transmission. Figure 3a presents the simulation results for the ferrite-only structure. The results indicate that the transmission coefficient $S_{21}$ remains near 0 dB across the entire frequency

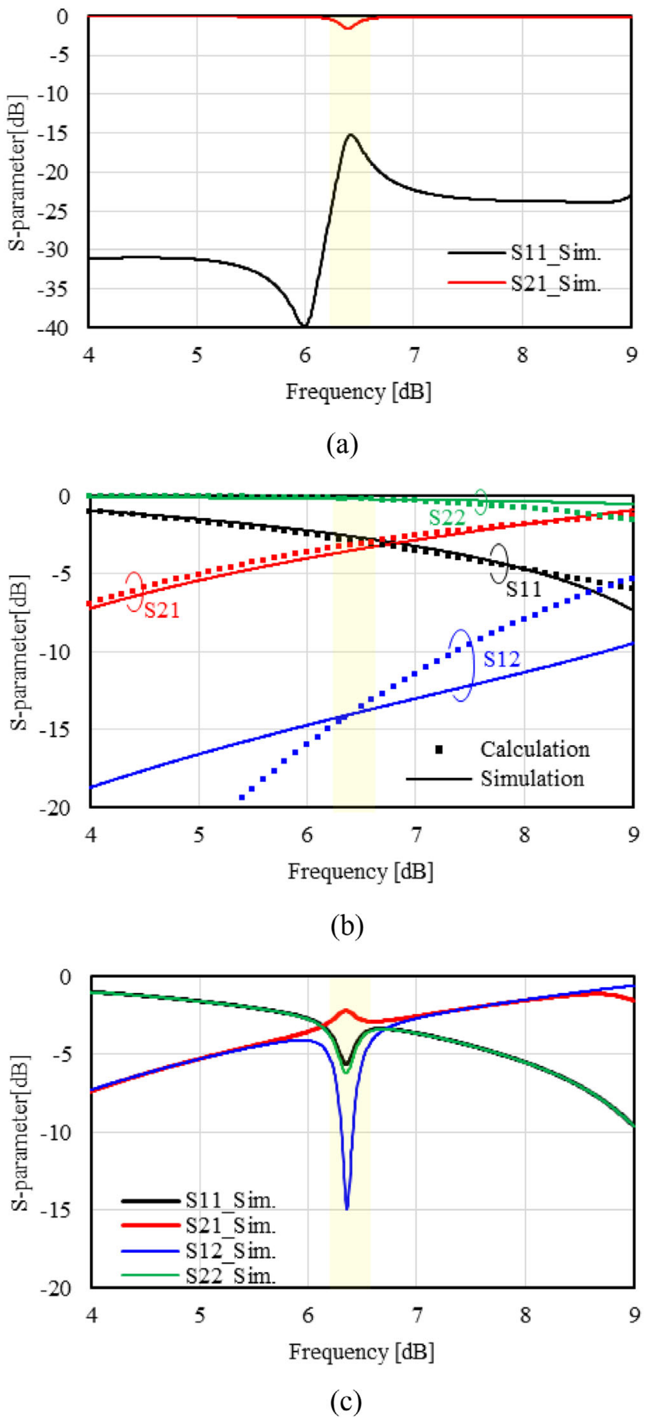


**FIGURE 3** | Design results of the nonreciprocal structure: comparison of electromagnetic field simulation and transmission line theory. (a) ferrite-only; (b) without ferrite; and (c) nonreciprocal structure.

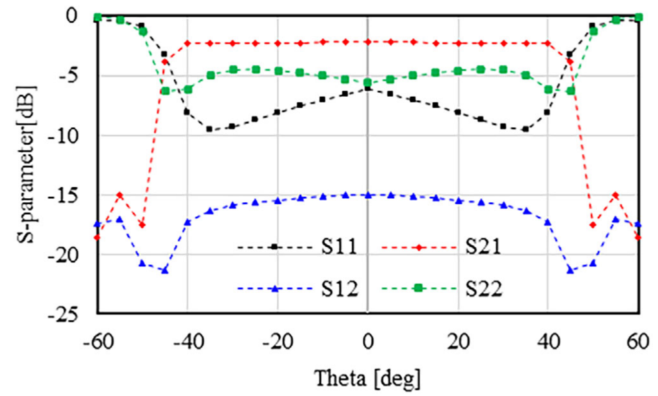


**FIGURE 4** | Theta angle characteristics of vertical polarization at 6.3 GHz.

band, demonstrating effective transmission. However, a slight dip in transmission is observed around 6.3 GHz. This reduction in $S_{21}$ is attributed to the rotational propagation within the ferrite, indicating the operating frequency band of the ferrite. Next, a comparison is made between the propagation characteristics calculated using the transmission line theory (Equations (2)–(7)) and the results from full-wave electromagnetic simulations. As shown in Figure 2, the proposed nonreciprocal structure consists of a ferrite disc with a metal strip on one side and an air gap on the other. For propagation from port 1, the ferrite's rotational behavior interacts with the metallic strip, resulting in a high-pass filter response. Specifically, the structure employs a metal strip array with a 30 mm pitch and an 11 mm line width. The theoretical $S_{11}$ and $S_{21}$ responses under this configuration are marked in Figure 3b. For comparison, full-wave simulation results for the structure shown in Figure 2d, excluding the ferrite, are also plotted as solid lines in Figure 3b, showing excellent agreement with the theoretical predictions. For excitation from port 2, the wave interacts with the air-gap side of the ferrite, effectively behaving as a structure with an equivalent-width air gap instead of a metal strip. This corresponds to a structure with a 30 mm pitch and a 19 mm line width. The calculated results for this case are marked as $S_{12}$ and $S_{22}$ in Figure 3b, alongside the corresponding simulation results. $S_{22}$ shows good agreement, while $S_{12}$ follows a similar trend to the theoretical prediction. Note that the equation used for the theoretical estimation (Equation (2)) is an approximation that yields more accurate results when the strip width is much smaller than the pitch; hence, the simulation results are considered more reliable.

Regardless, the high-pass characteristics for port 2 excitation are clearly shifted to higher frequencies compared to the port 1 case. Around 6.3 GHz—the ferrite's operational band—a stopband behavior is observed. Finally, Figure 3c presents the simulation results for the combined structure with ferrite and the metal strip array, as shown in Figure 2d. Outside the ferrite's operating band, the results closely match those of the metal strip-only case shown in Figure 3b, indicating minimal ferrite influence. Near 6.3 GHz, the port 1 transmission maintains the high-pass characteristics associated with the metal strip, while the port 2 transmission exhibits a sharp drop, confirming the stopband behavior. The peak suppression of $S_{12}$ reaches approximately–15 dB, consistent with the theoretical result shown in Figure 3b, confirming that the air-gap side effectively introduces nonreciprocal suppression when excited from port 2. These results demonstrate the advantage of the proposed structure in enabling nonreciprocity through post-design configuration, even after defining arbitrary metallic characteristics—an important feature for radome applications in antenna systems. The simulation results of the theta-angle characteristics in the horizontal plane for vertical polarization at 6.3 GHz, where nonreciprocity is observed, are shown in Figure 4. The plane wave response of the nonreciprocal structure,

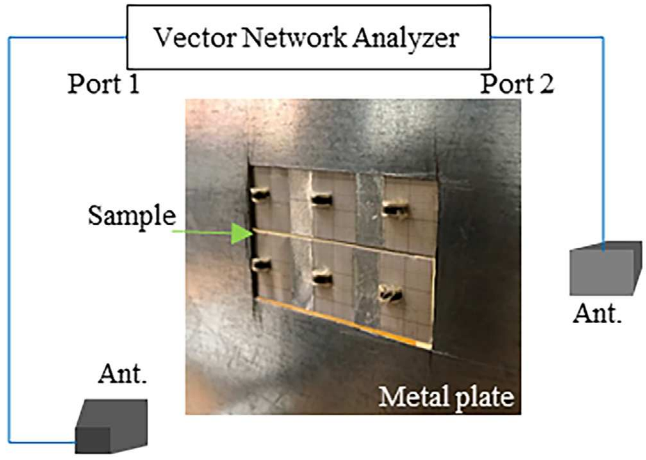


**FIGURE 5** | Measurement setup for nonreciprocal structure, showing antenna pair arrangement, metal plate with sample holes, and test configuration.

assuming an infinite plane, exhibits a similarity to the angular characteristics of a one-dimensional metal strip line. The results demonstrate that nonreciprocity can be achieved over a wide angular range exceeding ±40 degrees.

## 2.2 | Far-Field Measurements of Nonreciprocal Metasurfaces

Based on the design results, a prototype of the nonreciprocal structure was fabricated, and actual measurements were conducted. As discussed earlier, the proposed nonreciprocal structure is optimized for the wavelength, with the unit cell size comparable to the antenna dimensions. When employed as an antenna radome, this structure enables operation with one cell per antenna. Previous studies have demonstrated that the proposed nonreciprocal structure achieves characteristics equivalent to those of an infinite plane even when applied to a single cell or a finite number of cells [10, 16].

To account for potential interference from adjacent cells, a three-cell structure, incorporating left, center, and right cells, was utilized in the measurements. To realize an antenna with distinct transmission and reception patterns, two three-cell structures were prepared and positioned on the front and back sides of the antenna. For plane wave response characterization, these three cells were arranged in two rows, and the measurement setup is shown in Figure 5. A metal plate with holes was placed between two antennas to prevent reflections from the finite-sized sample. The holes were sized to match the 3-cell × 2-row configuration. Transmission characteristics, $S_{21}$ and $S_{12}$, were measured using a vector network analyser. The experimental results are compared with the electromagnetic field simulation in Figure 6.

The experimental measurements confirmed the nonreciprocal characteristics, with a peak at 6.3 GHz, consistent with the simulation results shown in Figure 3. While level fluctuations were observed in the experimental data due to reflections and interference from the mounting jig, the overall trends across the frequency band were consistent with the simulations. A specific drop around 5.5 GHz was attributed to interference with the sample holder, rather than an intrinsic issue with the design. These results confirm that the proposed nonreciprocal structure exhibits similar filter characteristics and nonreciprocity across the operating band, whether implemented as an infinite plane or a finite structure. Furthermore, the desired performance was achieved even in a three-cell antenna radome configuration.

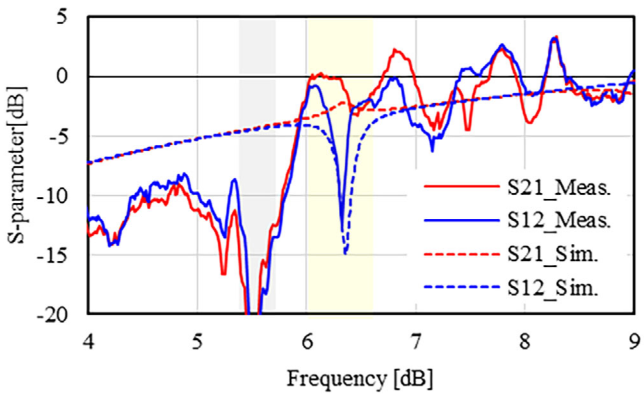


**FIGURE 6** | Comparison of experimental and simulation results for nonreciprocal structure.

# 3 | Antenna Design for Verifying Near-Field Characteristics

The monopole antenna used in this experiment exhibits isotropy in the horizontal xy-plane. A sleeve antenna, fabricated using a coaxial cable for ease of manufacturing, was employed as the monopole antenna. By utilizing an isotropic antenna in the horizontal plane, the effects on spherical waves in the near field can be evaluated. As shown in Figure 3, which presents the plane wave response results, the applied nonreciprocal metasurface exhibits a reflection component of approximately−6 dB in both the transmission and reflection directions. When used as a radome, an optimal placement distance is around 10 wavelengths; however, considering that the reflection component contributes to the antenna characteristics, the metasurface is positioned at approximately 1/4 wavelength. This placement allows for verification that the structure functions effectively as both a reflector and a radome. For the 6 GHz band, the antenna length was designed to be approximately 10 mm, corresponding to a quarter wavelength. An optimized sleeve antenna with a length of 9.7 mm was used in this study. Figure 7 illustrates the insertion characteristics of the designed sleeve antenna, with both simulation and experimental results confirming favorable performance at the operating frequency of 6.3 GHz. Using this antenna, the proposed structure was validated. It should be noted that, to account for the effect of the nonreciprocal metasurface on the radiation resistance when placed in proximity to the antenna, both simulations and measurements of $S_{11}$ were conducted with the metasurface in place. This approach ensures that the antenna is properly designed to operate in conjunction with the nonreciprocal metasurface.

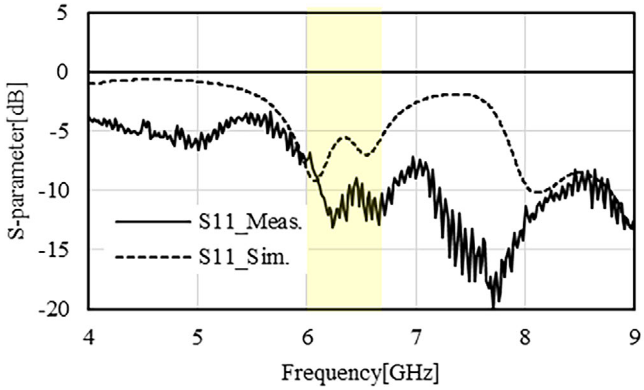


**FIGURE 7** | Insertion characteristics of the sleeve antenna.

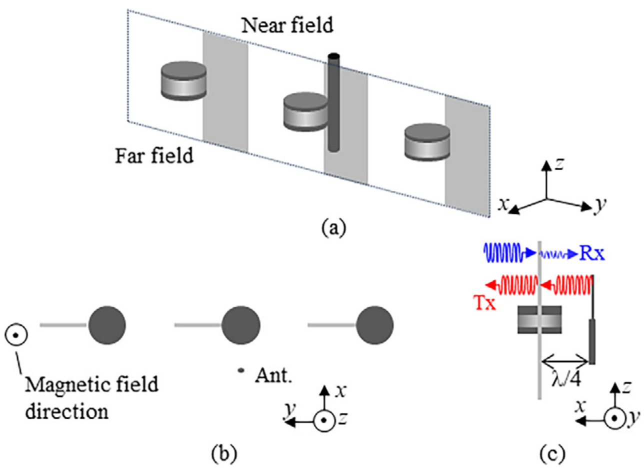


**FIGURE 8** | Structure of the null-point-forming antenna: (a) bird's-eye view; (b) top view; and (c) side view and operation overview.

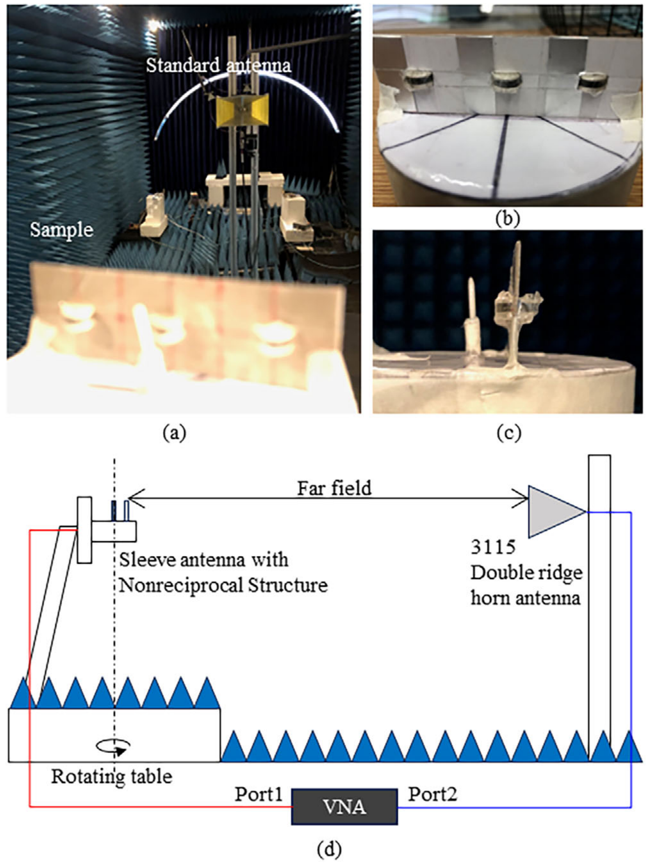


**FIGURE 9** | Experimental system for null-point-forming antenna: (a) overall experiment; (b) nonreciprocal structure; (c) side view of sample; and (d) overall measurement setup.

## 4 | Near Field Characteristic Verification

### 4.1 | Near Field Characteristics of the Front Radome

As the first step, we examined an antenna in which only the receiving pattern shows null points and the transmitting pattern remains isotropic. The antenna configuration under investigation is shown in Figure 8. As depicted in Figure 8a, this antenna characteristic, akin to a typical radome, relies on the near-field properties for propagation near the antenna, and the far-field plane-wave response for incoming signals from the opposite direction. Therefore, the nonreciprocal structure must exhibit consistent characteristics in both the near-field and far-field. To ensure proper operation, the antenna patterns of this structure were evaluated. The magnetic field orientation for nonreciprocal operation is shown in Figure 8b. Regarding the spatial relationship between the nonreciprocal structure and the antenna, as shown in Figure 8c, the structure is positioned approximately a quarter-wavelength away. While the exact quarter-wavelength separation is not critical for transmission properties, this distance is essential for forming beams in the reverse direction.

To obtain the characteristics of the null-point formation antenna, measurements were conducted using the setup shown in Figure 9. As illustrated in Figure 9a, the standard antenna used was a 3115 double-ridged horn antenna, and the sample was placed to ensure far-field separation. The sample, shown in Figure 9b, consisted of a three-cell unidirectional nonreciprocal structure arranged at a quarter-wavelength separation, as depicted in Figure 9c.

The experimental results are shown in Figure 10, along with the simulation results for comparison. Measurements were performed at the operational frequency of 6.3 GHz. In the results, the transmission patterns from the sample are indicated by red lines, the reception patterns by blue lines, and the patterns of the standalone antenna by green dashed lines. The results confirm the correct formation of null points near 0° in the forward direction of the antenna equipped with the nonreciprocal structure. A comparison of the experimental and simulation results revealed that the angles at which null points formed, and the angular range over which nonreciprocity occurred were similar. This agreement confirms that the expected nonreciprocity characteristics were successfully achieved. A notable observation is that sharp null points were formed over an angular range of approximately ±5°, while angular regions with noticeable differences between the red and blue lines extended over 50°. This indicates that the cylindrical ferrite exhibits no angular variation in its circumferential characteristics, enabling the ferrite's rotational propagation properties, which are the basis for nonreciprocity, over a wide angular range. The nonreciprocity angular range was found to be similar to the far-field characteristics shown in Figure 4. In

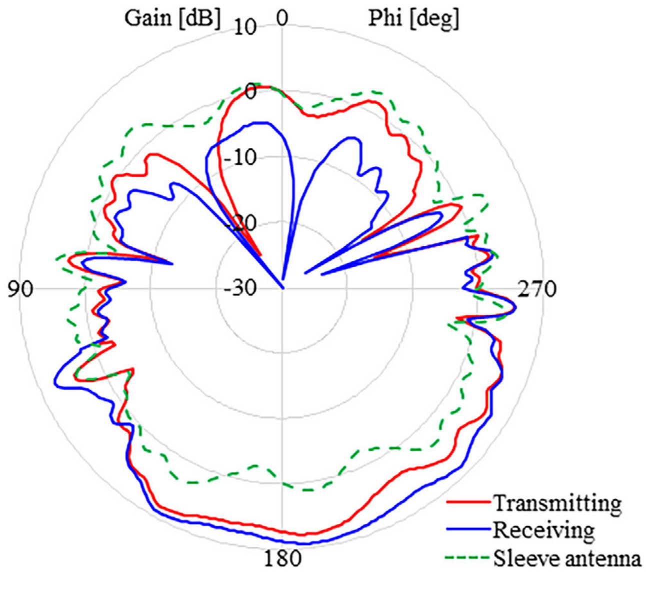


(a)

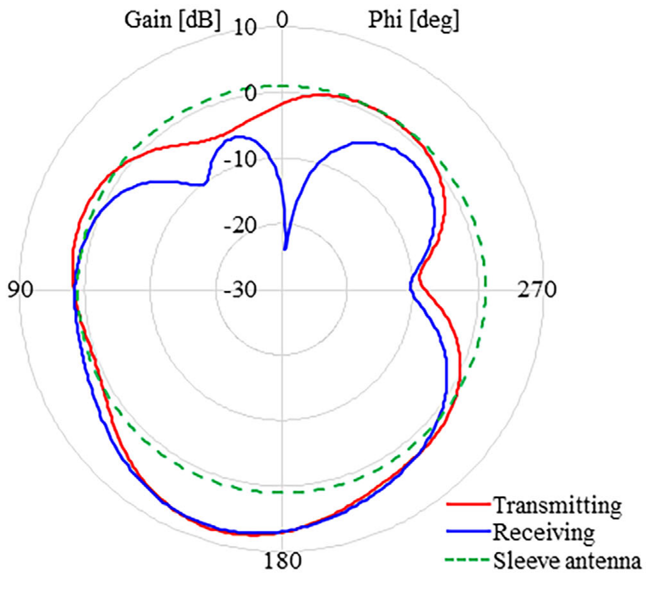


(b)

**FIGURE 10** | Antenna pattern of null-point-forming antenna: (a) experimental results; and (b) simulation results.

the experiment, dips occurred in certain angular ranges due to the influence of the surrounding structure. However, dips were also observed in the pattern of the sleeve antenna alone, which is attributed to the effect of the antenna mounting jig and other factors. When using a unidirectional nonreciprocal structure, the pattern on the side opposite the null-point direction exhibited higher gain than the sleeve antenna alone, indicating that the structure also acted as a reflector. These results demonstrate that null points can be created in the reception pattern to reduce interference with nearby antennas while maintaining the transmission pattern. Furthermore, the proposed nonreciprocal structure allows for reversing the transmission and reception

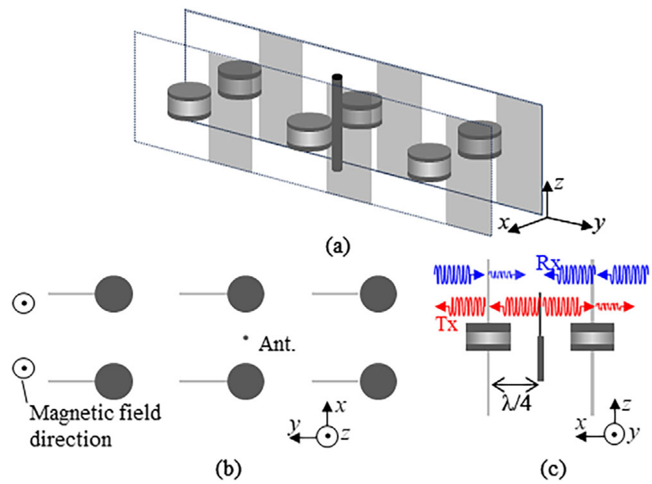


**FIGURE 11** | Structure of separate transmission and reception pattern antenna: (a) bird's-eye view; (b) top view; and (c) side view, and operation overview.

patterns by simply changing the magnetic field orientation, enabling easy control of null points.

### 4.2 | Double-Sided Nonreciprocal Radome Structure

Next, we verify the effect of placing nonreciprocal metasurfaces on both the front and back of the antenna. Similar to the previous radome, nonreciprocal structures were placed near the sleeve antenna; however, they were arranged at the front and rear at a separation of a quarter wavelength. Figure 11 illustrates the model configuration. As shown in Figure 11a and b, the orientations of the metal strips and magnetic fields were aligned in the same direction for the front and rear structures. This configuration achieves nonreciprocity in the same direction, enabling the formation of null points in different directions for transmission and reception. Note that, due to the asymmetry of the metal orientation with respect to the x-axis, the antenna pattern in the 90° and 270° directions also becomes asymmetric with respect to the x-axis. To address this asymmetry, the metal positions can be arranged in rotational symmetry between the front and rear structures, but this requires reversing the magnetic field direction between the two structures.

To verify the characteristics of this antenna, we conducted measurements. Figure 12 shows the antenna sample and experimental setup. The positional relationship between the standard antenna and the sample is depicted in Figure 12a. Figure 12b and c show a structure where three nonreciprocal cells were arranged at the front and rear with a quarter-wavelength separation. The purpose of this structure is to achieve the operation depicted in Figure 11c, where only the transmitted signal (red line) passes in the forward direction (positive x-axis), while only the received signal (blue line) passes in the backward direction (negative x-axis).

The experimental results, presented in Figure 13, are compared with the simulation results. The transmission pattern exhibited a main beam in the 0° direction and a gain dip in the 180° direction. Conversely, the reception pattern showed a main beam

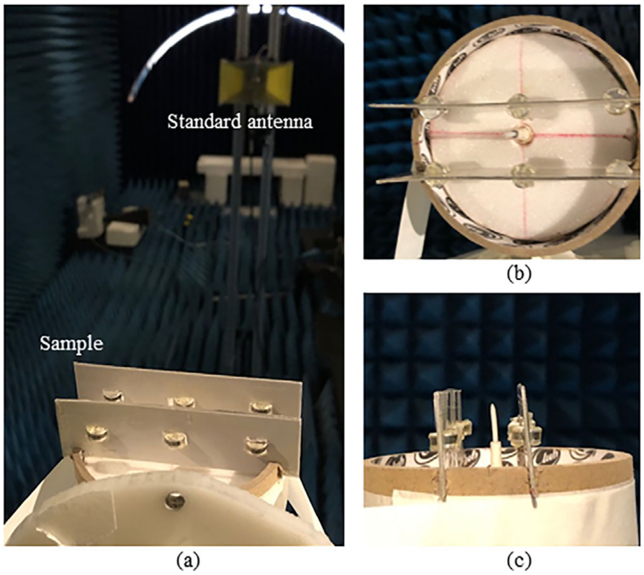


**FIGURE 12** | Experimental system for transmitting and receiving pattern antennas: (a) overall experiment diagram; (b) top view of the sample; and (c) side view of the sample.

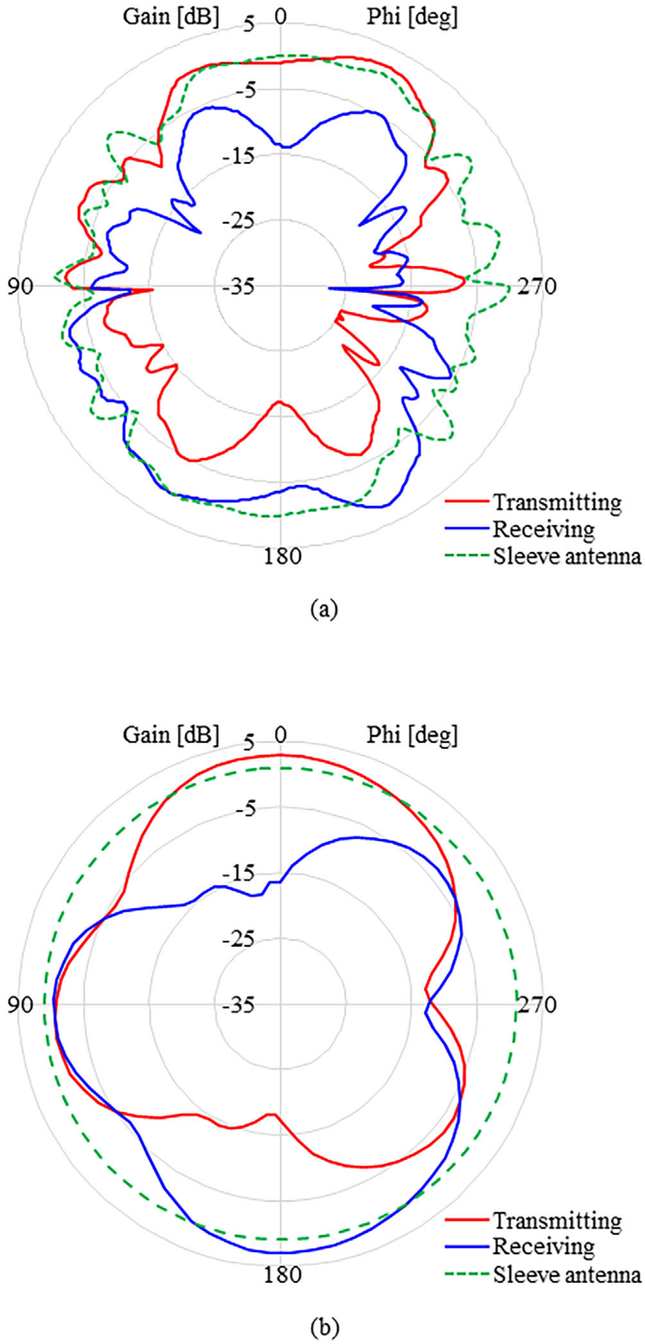


**FIGURE 13** | Antenna patterns for transmitting and receiving pattern antennas: (a) experimental results; and (b) simulation results.

in the 180° direction and a gain dip in the 0° direction. The main beam demonstrated a gain comparable to that of the sleeve antenna alone, confirming accurate nonreciprocal characteristics. Furthermore, when two nonreciprocal structures were placed at the front and rear, the antenna pattern exhibited broader nonreciprocal coverage compared to using only one structure, albeit with slightly reduced sharpness. This broad coverage is likely due to the combined influence of the nonreciprocal structures acting as reflectors, which expanded the angle range of nonreciprocity. Both the experimental results (Figure 13a) and simulation results (Figure 13b) revealed radiation in the 90° direction and dips in the 270° direction. This trend relates to the positions of the metal strips and air gaps in the nonreciprocal structure: radiation occurs in the 90° direction due to the presence of metal strips, whereas dips occur in the 270° direction where the ferrite is visible. As observed in the case of placement on the front side, the experiment showed some drops around 90 degrees and 270 degrees due to the influence of the antenna holder. Despite these drops, the characteristics in the main azimuth directions of 0 degrees and 180 degrees remained relatively consistent, highlighting the usefulness of simulations in the design process.

### 4.3 | Radome Nonreciprocity Control

One advantage of this structure is its ability to control the formation of multiple null points, even when nonreciprocal structures are placed in front of and behind the antenna. The one-dimensional metal strip structure combined with ferrite exhibits high-pass filter characteristics, ensuring minimal impact on the antenna pattern even when positioned nearby. In other words, if the ferrite is not magnetized, the antenna can function like a standard antenna despite the presence of a nonreciprocal structure. The magnetization state of the ferrite can be switched by attaching or detaching permanent magnets or by toggling an electromagnet. Our group has achieved nonreciprocal characteristics using an electromagnet of the same size as the permanent magnet employed in the experiments [13], indicating that the proposed structure in this study can also utilize this approach for control. Electromagnetic field simulation results illustrate the patterns in the non-magnetized and partially magnetized states. First, consider the pattern when nonreciprocal structures are placed but remain unmagnetized, as shown in Figure 14a. In this state, the antenna is expected to exhibit a uniform pattern in the horizontal plane due to simple transmission characteristics, despite the presence of nearby nonreciprocal structures. The simulation results, represented by the green dashed line in Figure 14c, reveal that while characteristic points appear at 90° and 270° due to the structure, the pattern at the 0° and 180°

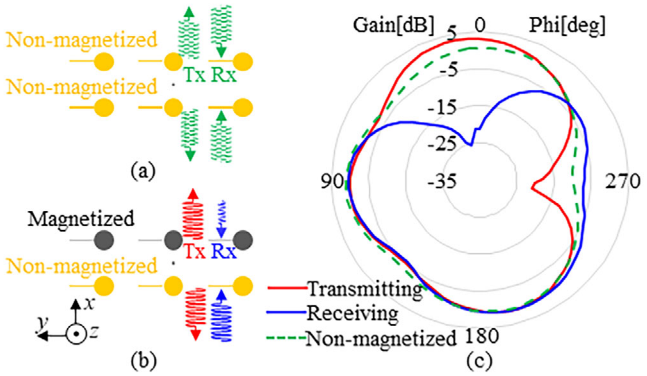


**FIGURE 14** | Example of pattern control: (a) model with non-magnetized both sides; (b) model with magnetized only one side; and (c) simulation results.

directions aligns closely with that of the antenna alone. Next, examine the scenario where only one side of the structure is magnetized, as depicted in Figure 14b. This analysis focuses on magnetizing the nonreciprocal structure in the forward 0° direction. In this case, the antenna can form a null point in the reception pattern while maintaining the transmission pattern, similar to the null point-forming antenna.

### 4.4 | Application to Array Antennas

As previously discussed, the proposed structure features unit cell sizes comparable to the antenna dimensions, demonstrating that effective performance can be achieved with a single cell [16]. This characteristic enables the expansion of the structure to an array antenna, where adjacent antennas are spaced according to the cell size. While the previously demonstrated separate pattern antennas were limited to operation within a horizontal plane, extending the concept to a two-dimensional array can realize antennas with separate transmission and reception patterns in three-dimensional space. To verify this, a two-dimensional array antenna composed of $4 \times 4$ elements was modeled, with antenna elements spaced at intervals equal to the unit cell size, as shown in Figure 15a. Simulations synthesized beam patterns based on the results shown in Figure 13b. The analysis results for beam scanning in the 0° direction are illustrated in Figure 16, while those for beam scanning in the 10° Phi direction are presented in Figure 17. Figure 16a depicts the horizontal plane results, and Figure 16b shows the three-dimensional beam patterns. The simulations confirmed that the main transmission lobe aligns with the 0° direction and the main reception lobe aligns correctly with the 180° direction. Even within the side lobes—falling within the angular range of nonreciprocity for a single element—transmission and reception exhibit differences, but isolation exceeding 10 dB is consistently achieved at the main lobe. Beam scanning is constrained to angles within the range where nonreciprocity is effective. Figure 17 shows the results of beam scanning at 10° in the horizontal plane. Even with scanning, the main lobe achieves the highest isolation, maintaining robust separation. Due to the relationship between phase control, a transmission main lobe at 10° results in a reception main lobe at 170°. For a two-dimensional array placed in the yz-plane, the results exhibit symmetry with respect to the zx-plane. These

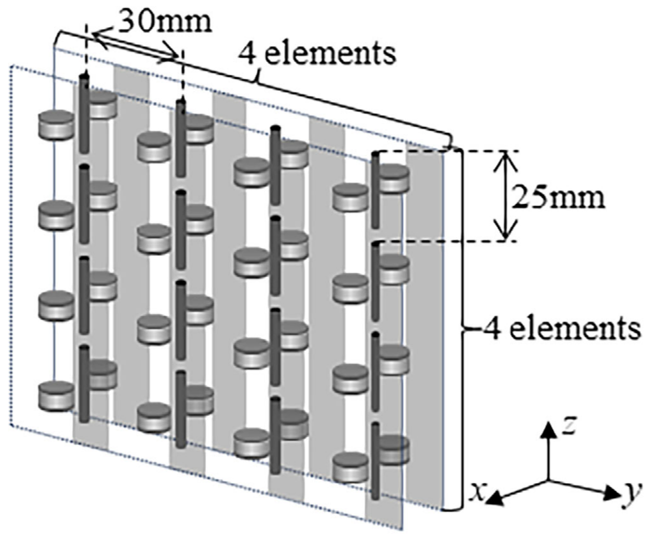


**FIGURE 15** | Model for $4 \times 4$ array analysis.

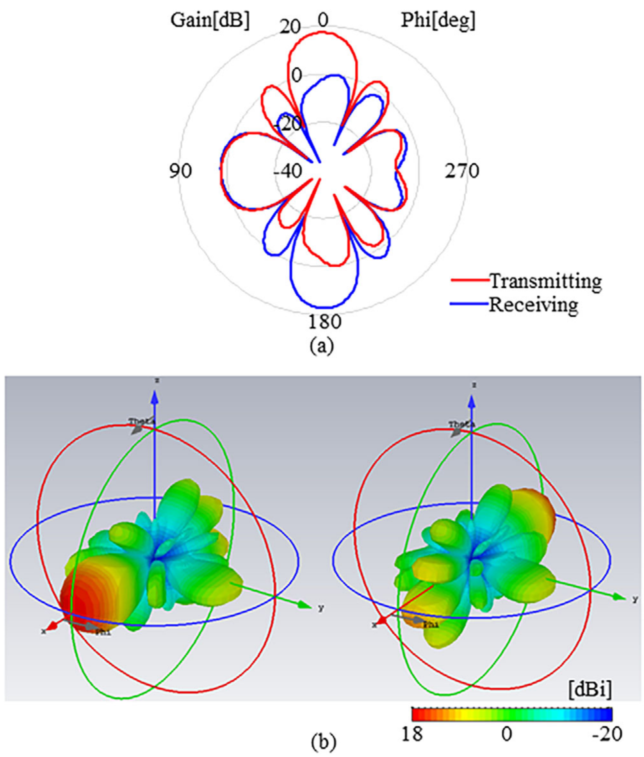


**FIGURE 16** | Simulation results pointing in the zero-degree direction: (a) antenna pattern in horizontal plane; and (b) transmitting pattern (left) and receiving pattern (right).

results demonstrate that the proposed separate transmission and reception pattern antenna is applicable to both single-element antennas and array antennas. Moreover, it can be extended to include beam scanning applications, showcasing its versatility and scalability.

## 5 | Conclusion

As a measure to mitigate electromagnetic interference originating from the antenna, we verified the effectiveness of a nonreciprocal

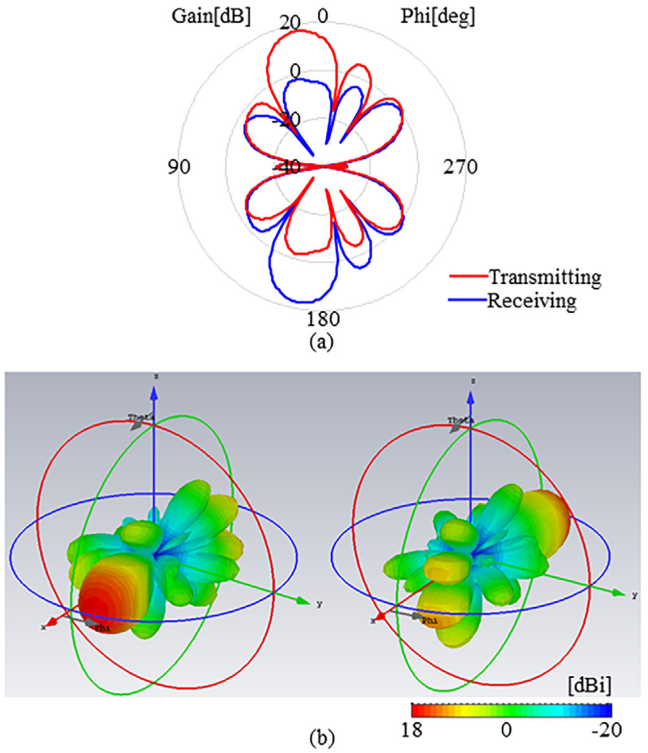


**FIGURE 17** | Simulation results pointing in the 10-degree direction, (a) antenna pattern in horizontal plane; and (b) transmitting pattern (left) and receiving pattern (right).

metasurface positioned and operating in close proximity to the antenna. It is now possible to physically form null points in the transmitting or receiving patterns, enabling new applications such as suppressing radiation in a specific direction while maintaining isotropic reception. In this study, for a nonreciprocal metasurface with an isolation of 10 dB or more at 6.3 GHz, we established its effect on the near-field pattern, which becomes a spherical wave, as well as its plane-wave response. These effects were verified through experiments and simulations, including the design methodology. The scalability of this antenna configuration was also highlighted, as it can be adapted to various frequency bands by adjusting the ferrite properties and unit-cell design.

## Author Contributions

**Kazuhiro Takahagi:** conceptualization, data curation, formal analysis, methodology, project administration, validation, visualization, and writing – original draft preparation. **Alan Tennant:** funding acquisition, investigation, resources, software, supervision, and writing – review & editing.

## Conflicts of Interest

The authors declare no conflicts of interest.

## Data Availability Statement

The data that support the findings of this study are available from the corresponding author upon reasonable request.

## References


1. Q.-F. Liu, S.-Q. Zheng, Y. Zuo, H.-Q. Zhang, and J.-W. Liu, "Electromagnetic Environment Effects and Protection of Complex Electronic Information Systems," in *2020 IEEE MTT-S International Conference on Numerical Electromagnetic and Multiphysics Modeling and Optimization (NEMO)* (2020): 1–4, https://doi.org/10.1109/NEMO49486.2020.9343630.

2. J. Zheng and G. Wei, "New Development of Electromagnetic Compatibility in the Future: Cognitive Electromagnetic Environment Adaptation," in *2011 13th Global Symposium on Millimeter-Waves & Terahertz (GSMM)* (2021): 1–3, https://doi.org/10.1109/GSMM53250.2021.9511983.

3. H. Sun and Y. Qin, "Stealthy Configuration Optimization Design and RCS Characteristics Study of Microsatellite," *Aerospace* 9, no. 12 (2022): 815.

4. X. Chen, V. Savaux, M. Crussière, P. Savelli, and K.-C. Yao, "Constrained-MMSE Combining for Spatial Domain Self-Interference Cancellation in Full-Duplex Massive MIMO Systems," *IEEE Open Journal of the Communications Society* 5 (2024): 649–663.

5. G. Byun, H. Choo, and S. Kim, "Design of a Small Arc-Shaped Antenna Array With High Isolation for Applications of Controlled Reception Pattern Antennas," *IEEE Transactions on Antennas and Propagation* 64, no. 4 (2016): 1542–1546.

6. M. N. Anwar Tarek, M. Roman, and E. A. Alwan, "Power Efficient RF Self-Interference Cancellation System for Simultaneous Transmit and Receive," in *2021 IEEE International Symposium on Antennas and Propagation and USNC-URSI Radio Science Meeting (APS/URSI)* (2021): 113–114, https://doi.org/10.1109/APS/URSI47566.2021.9704722.

7. T. Lou, X.-X. Yang, G. He, W. Che, and S. Gao, "Dual-Polarized Nonreciprocal Spatial Amplification Active Metasurface," *IEEE Antennas and Wireless Propagation Letters* 20, no. 9 (2021): 1789–1793.

8. S. Y. Wang, Q. W. Zhang, X. H. Zhang, and Y. B. Li, "The Design of Wideband Nonreciprocal Transmission by Active Metasurface," *IEEE Antennas and Wireless Propagation Letters* 22, no. 8 (2023): 2012–2016.

9. A. Parsa, T. Kodera, and C. Caloz, "Ferrite Based Non-Reciprocal Radome, Generalized Scattering Matrix Analysis and Experimental Demonstration," *IEEE Transactions on Antennas and Propagation* 59, no. 3 (2011): 810–817.

10. K. Takahagi and A. Tennant, "Experimental Verification of Nonreciprocal Electromagnetic Metasurface in a Finite-Size Array," *Electronics Letters* 60, no. 12 (2024): e13240.

11. W. Yang, J. Qin, J. Long, et al., "A Self-Biased Non-Reciprocal Magnetic Metasurface for Bidirectional Phase Modulation," *Nature Electronics* 6 (2023): 225–234.

12. A. Ashley, L. F. Marzall, M. Pinto, Z. Popovic, and D. Psychogiou, "Bandwidth Design of Ferrite-Based Circulators," in *2018 International Applied Computational Electromagnetics Society Symposium (ACES)* (2018): 1–2, https://doi.org/10.23919/ROPACES.2018.8364118.

13. K. Takahagi and A. Tennant, "Nonreciprocal Metasurfaces Analyzing Temperature Characteristics," in *2024 18th European Conference on Antennas and Propagation (EuCAP)* (2024): 1–4, https://doi.org/10.23919/EuCAP60739.2024.10501100.

14. Trans-Tech, "A Subsidiary of Skyworks Solutions, Inc.," Products for RF/Microwave Applications; Microwave garnets: Products catalogue, pages 66–80, https://datasheet.octopart.com/SR9000SPQ0472AY-Trans-Tech-datasheet-8861441.pdf.

15. D. M. Pozar, *Microwave Engineering*. 4th ed. (New York, NY, USA: John Wiley and Sons, 2012): 451–464.

16. K. Takahagi and A. Tennant, "Experimental Validation of Nonreciprocal Metasurface Using Simple Structure," *The Journal of Engineering, Issue* 10 (2024): e70011.